Volume 3 | Number 25 | 7 July 2015 | Pages 13097–13580

Journal of Materials Chemistry A

Materials for energy and sustainability

www.rsc.org/MaterialsA

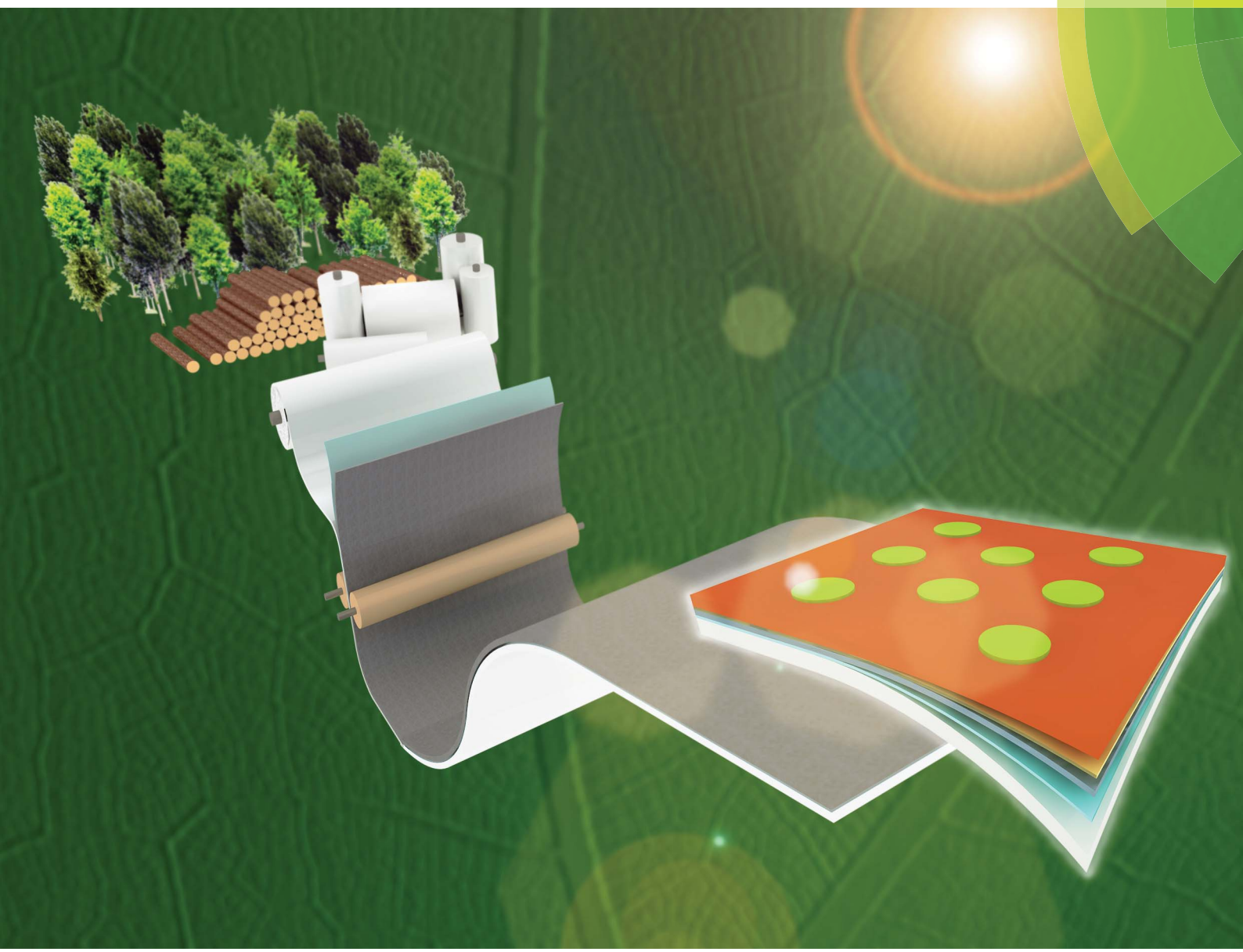

ISSN 2050-7488

ROYAL SOCIETY OF CHEMISTRY

PAPER

António Vicente, Rodrigo Martins *et al.*

Solar cells for self-sustainable intelligent packaging

Journal of Materials Chemistry A

PAPER

View Article Online
View Journal | View Issue

Cite this: J. Mater. Chem. A, 2015, 3, 13226

Solar cells for self-sustainable intelligent packaging†

António Vicente,*[a] Hugo Águas,[a] Tiago Mateus,[a] Andreia Araújo,[a] Andriy Lyubchyk,[a] Simo Siitonen,[b] Elvira Fortunato[a] and Rodrigo Martins*[a]

Received 10th March 2015
Accepted 17th March 2015

DOI: 10.1039/c5ta01752a

www.rsc.org/MaterialsA

Nowadays there is a strong demand for intelligent packaging to provide comfort, welfare and security to owners, vendors and consumers by allowing them to know the contents and interact with the goods. This is of particular relevance for low cost, fully disposable and recyclable products, such as identification tags and medical diagnostic tests, and devices for analysis and/or quality control in food and pharmaceutical industries. However, the increase of complexity and processing capacity requires continuous power and can be addressed by the combined use of a small disposable battery, charged by a disposable solar cell, which is able to work under indoor lighting. Herein, we show a proof-of-concept of the pioneering production of thin-film amorphous silicon (a-Si:H) solar cells with an efficiency of 4% by plasma enhanced chemical vapour deposition (PECVD) on liquid packaging cardboard (LPC), which is commonly used in the food and beverage industries. Such accomplishment put us one step closer to this revolution by providing a flexible, renewable and extremely cheap autonomous energy packaging system. Moreover, such Si thin films take advantage of their good performance at low-light levels, which also makes them highly desirable for cheap mobile indoor applications.

1. Introduction

Traditional packaging has deeply contributed to increase the shelf life of food and beverage and to improve the food distribution systems. However, with the increasing complexity of today's society, adding value to packaging has become a priority, namely, to address the consumer's needs of natural products with less additives, higher regulation and quality control, to assure food safety,[1] and a fast and optimized distribution process.

Micro-technologies and nano-technologies (MNTs) can be the key to address such demands[2] by imparting the package with the ability to acquire, store and transfer data (smart packaging)[3] and to even communicate and carry out logic functions to take decisions (intelligent packaging)[4] and, at the same time, provide low cost solutions.[5] For this reason, it is estimated that in the next decade, nanotechnology will have an impact of 25% on the food packaging market, currently valued at $100 billion.[6]

The strategy to achieve such impact will involve the production of self-sustained systems that comprise the integration of several functionalities into one single device, such as environmental monitoring,[4] stock tracking[7] and package integrity/tampering,[8] together with features like emissive or reflective digital displays[9,10] or self-heating or self-cooling packages,[11] which in turn will demand smart hybridization solutions that combine printed electronics[12] (more cost efficient for large area integration) and silicon technologies (more cost effective per function, such as high-performance communication and advanced processing).[13] Combining printed batteries with a power generator, such as the a-Si:H solar cells described herein, unlocks the spectrum of possible package solutions with incredible added value at a low cost.

Recently, the production of solar cells on cellulose-based substrates has gained significant attention due to the noteworthy developments.[14–18] Its roughness can be advantageous for solar cells as it may contribute to light trapping. In addition, it also poses key challenges to its practical use, since cellulose has a relatively low tolerance to temperature and can release some contaminants to both the deposition reactor and the deposited solar cell. Its natural porosity can also favor such release and lower the shunt resistance of the cells (due to short-circuiting). The use of low process temperatures, relative to those ($\gtrsim$200 °C) typically employed in processing solar cells with high efficiencies,[19] is crucial to avoid substrate damage. Moreover, such challenges are not crucial for organic solar cells, as they do not require high temperature or vacuum methods.

[a]CENIMAT/I3N, Departamento de Ciência dos Materiais, Faculdade de Ciências e Tecnologia, FCT, Universidade Nova de Lisboa and CEMOP/UNINOVA, 2829-516 Caparica, Portugal. E-mail: amv17109@campus.fct.unl.pt; rm@uninova.pt; Fax: +351 212941365; Tel: +351 212948525

[b]Stora Enso Oyj, Renewable Packaging, Research Centre Imatra, Tornansaarenraitti 48, 55400 Imatra, Finland

† Electronic supplementary information (ESI) available: Experimental details and preliminary results: fabrication and characterization of silicon thin films; liquid packaging cardboard surface analysis: Optical Emission Spectroscopy (OES); design of experiment and mathematical modeling (DoE); Influence on the solar cell properties of performing hydrogen plasma treatment on the substrate; Quadrupole Mass Spectroscopy (QMS). See DOI: 10.1039/c5ta01752a

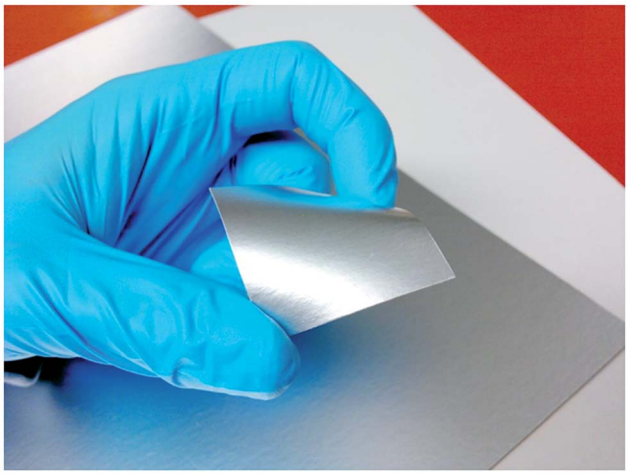

Fig. 1 Image of the Liquid Packaging Cardboard (LPC) substrate used for a-Si:H solar cell deposition.

However, their low efficiencies (~2%) and poor environmental stability still pose considerable limitations to the viability of such organic approaches.[15,20,21]

The solar cells developed in this study were produced on a packaging cardboard, named "Lunchbox",[22] composed of three layers: (1) the cardboard (with a density of 240 g m^{-2}), consisting of pressed cellulose fibers, which provides mechanical support and resistance to the device, (2) the adhesive layer of low density polyethylene, LDPE (12 g m^{-2}), essential in the lamination process, and (3) the aluminium sheet (6–7 μm), which serve as the rear contact and reflective layer (Fig. 1).

Furthermore, the usage of liquid packaging cardboard (LPC) has environmental advantages, as cellulose comes from sustainable organic sources hence minimizing the environmental impact of such packages, as well as industrial advantages, since it is compatible with roll-to-roll technologies (also the preferred manufacturing process used in packaging industry[13]), making it ideal for mass production of solar cells on low cost flexible and disposable substrates for intelligent packaging applications.

2. Experimental details

2.1 Substrate cleaning and characterization

The reference glass substrates were sequentially cleaned with soap, deionized water, acetone (ultrasonic bath), deionized water and isopropanol (ultrasonic bath). After cleaning, the substrates were dried using N_2. The liquid packaging cardboards were cleaned solely with a polyester/cellulose blend wiper (which does not leave residues behind) wetted with isopropanol, dried using N_2 and baked at 155 °C for 12 h.

The LPC surface was analyzed by optical spectroscopy, 3D profilometry and SEM in order to evaluate the metal reflectance, roughness and presence of defects, respectively. Reflectance measurements were obtained in a double beam UV-VIS-NIR Shimadzu spectrophotometer with an integrating sphere. Surface 3D profilometry was performed using an Ambios XP-200 profiler (USA) with a 3 μm line spacing for an area of 3 × 2 mm and the software data compilation from TrueMap. SEM observations were carried out using a Carl Zeiss AURIGA CrossBeam (FIB-SEM) workstation equipped for EDS measurements. For the FIB experiments, which were performed to observe the inner cross section of the solar cell, Ga^+ ions were accelerated to 30 kV at 100 pA and the etching depth was maintained at around 800 nm. A thin layer (~30 nm) of carbon was deposited on the material surface to minimize Ga contamination. Differential scanning calorimetry (DSC) and thermogravimetric analysis (TGA) were carried out in a simultaneous thermal analyser (TGA-DSC-STA 449 F3 Jupiter) at atmospheric pressure. Approximately 21 mg of LPC was loaded into an aluminium pan and heated from 40 to 425 °C at a heating rate of 5 °C min^{-1}.

2.2 Fabrication and characterization of the solar cells

Hydrogenated amorphous silicon (a-Si:H) thin film solar cells were deposited by high frequency (27.12 MHz) plasma enhanced chemical vapour deposition (HRF-PECVD) in a single-chamber reactor on glass and LPC substrates with an area of 40 × 40 mm^2.

For the reference glass substrate, the first step was the deposition of Al back contact (200 nm) evaporated in vacuum (10^{-6} mbar) using an e-beam system. The following step, common to both substrates, was the growth of a thin AZO (Al_2O_3: 2 wt%, ZnO: 98 wt%) layer with ~60 nm deposited by RF-magnetron sputtering at 155 °C. The AZO resistivity is in the order of $\rho = \sim 5 \times 10^{-3}$ Ω cm. The samples were then transferred to the PECVD system wherein the silicon layers were deposited according to the n–i–p structure. A mixture of SiH_4 and H_2 defines the hydrogen dilution parameter (D_H (%) = [H_2/(H_2 + SiH_4)] × 100). In the case of the intrinsic silicon thin film, D_H = 80% and a gas pressure (P_{gas}) of 0.4 Torr and a power density (P_W) equal to 21 mW cm^{-2} were used. Adding trimethylboron (TMB, $B(CH_3)_3$) and PH_3 to the mixture of SiH_4 and H_2 produced p- and n-layers, respectively. p-a-Si:H has a D_H = 92%, R_{TMB} = TMB/(TMB + SiH_4) = 0.68% and was deposited at P_{gas} = 1.0 Torr, P_W = 15 mW cm^{-2}; moreover, as for the n-a-Si:H thin film, the parameters are: D_H = 79%, R_{PH_3} = PH_3/(PH_3 + SiH_4) = 0.26%, P_{gas} = 0.4 Torr, P_W = 21 mW cm^{-2}. More information regarding Si films deposition can be found in ESI Table S1 and S2.†

The electrical properties of the films were studied *via* temperature dependent dark conductivity, from which the room-temperature conductivity ($\sigma_{d@25\ °C}$) and activation energy (E_a) were calculated. The linearity of the $I(V)$ dependence was confirmed before each conductivity measurement. Low voltages (0.1–1 V) were used to reduce the high-field effects such as field-enhanced hopping transport. Coplanar aluminium contacts (200 nm thick, 4 mm long and 1 mm apart) were deposited over the Si active layer by electron beam evaporation.

Lastly, the top-contact IZO (In_2O_3: 89.3 wt%, ZnO: 10.7 wt%), a transparent conductive oxide with a resistivity in the range of $\rho = \sim 5 \times 10^{-4}$ Ω cm, was deposited by RF-magnetron sputtering at room temperature employing a 25 × 25 mm polyimide mechanical mask with open circles (2.5 mm diameter) to define the cell areas of ~5 mm^2.

The solar cells were characterized by current–voltage (J–V) measurements at room temperature under AM1.5 (100 mW cm^{-2}) light conditions in a Spire Sun Simulator 240A and the external quantum efficiency (EQE) of the cells was determined in short-circuit condition in the wavelength range of 360 to 1100 nm using a home-made set up.[23]

Quadrupole Mass Spectrometry (QMS) real-time process data were collected using a mass spectrometry system (EXtorr, model XT100M) mounted parallel to the process chamber exhaust line and the exhaust gases were collected through a 10 μm sampling orifice located 500 mm away from the outer edge of the RF electrode for a detection mass range up to 100 amu. Optical Emission Spectroscopy (OES) was used to collect the plasma-emitted light through a photo-collimator placed at a quartz viewport of the reactor (to ensure the recording of total emission of the plasma – from bulk and sheaths) and guided by the optical fiber to an Ocean Optics HR4000 spectrometer with a spectral range of 200 to 1100 nm.

3. Results and discussion

The fabrication strategy presented herein is able to address the challenges described in the introduction not only by achieving a good compromise between the deposition conditions, which is indispensable to obtain an homogeneous coverage of the surface and high quality Si active layers; but also by continuously monitoring the deposition process *via* optical emission spectroscopy and mass quadrupole spectrometry, tools which control the paper degasification and species present in the deposition chamber. To optimize the cell's layer structure, a fast approach through a design of experiment (DoE) tool was also applied to obtain layers with adequate thickness and electro-optical characteristics (see ESI Fig. S2–S4 and Tables S3–S7†).

3.1 Liquid packaging cardboard surface characteristics

Fig. 2 depicts the surface characterization performed on the LPC. Fig. 2a shows that the LPC has a highly rough surface with a root mean square (RMS) value of almost 6 μm. The substrate's reflectivity (Fig. 2b) is around 80% and constant over the entire range of visible spectrum (300 to 800 nm) and the diffuse reflection (R_d) contributes with the biggest fraction to the total reflection (R_t), wherein $R_t = R_d + R_s$ (specular reflection). Between 300 and 380 nm, the total reflection (R_t) is even higher compared to a 200 nm Al film deposited on glass.

Differential scanning calorimetry was then used to determine the thermal properties of LPC. Fig. 3 depicts the thermogravimetry (TG) and temperature-dependent heat flux (blue dash line) results for laminated cardboard substrates (sample mass: 21 mg). The endothermic peak detected at 99.3 °C, with a weight loss of 6.6% ("A" on Fig. 3), indicates the release of adsorbed water. Due to the low melting temperature of LDPE,[24] LPC decomposition occurs at 200 °C. However, up to 250 °C, the weight loss is negligible. At temperatures above 250 °C, a mass loss of 57.7% ("B" on Fig. 3) occurs, followed by rapid substrate decomposition.[25,26] Thus, the substrate is thermally stable up to 200 °C and possibly viable up to 250 °C.

Given the intrinsic roughness of the cardboard coupled with the high reflectivity of the aluminium layer, the surface is free of fissures and is thermally stable at the required low temperature of ~150 °C; moreover, one can be confident of the substrate viability for functional silicon thin film solar cells deposition.

3.2 The fabrication process of solar cells on liquid packaging cardboard (LPC)

Fig. 4a highlights the process steps required to produce solar cells on LPC. Fig. 4b shows a highly rough surface but free of cracks and Fig. 4c is a SEM image of the solar cells cross section

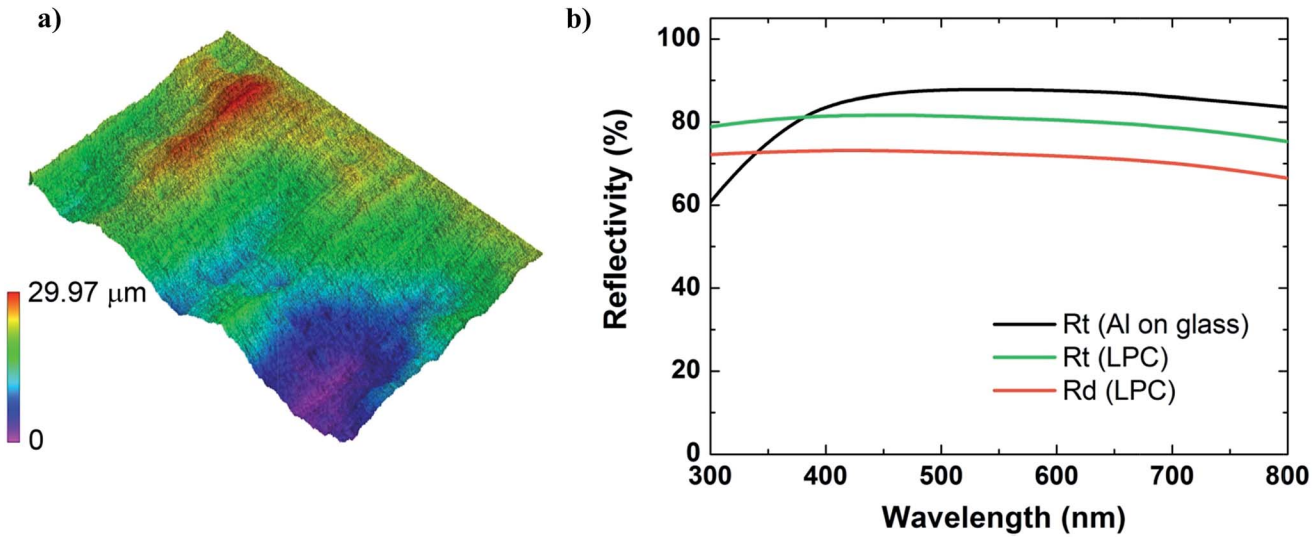

Fig. 2 Surface characterization analysis. (a) 3D profilometer on a 3 × 2 mm area; (b) total (R_t) and diffuse (R_d) reflection in the visible region of LPC and glass coated with aluminium.

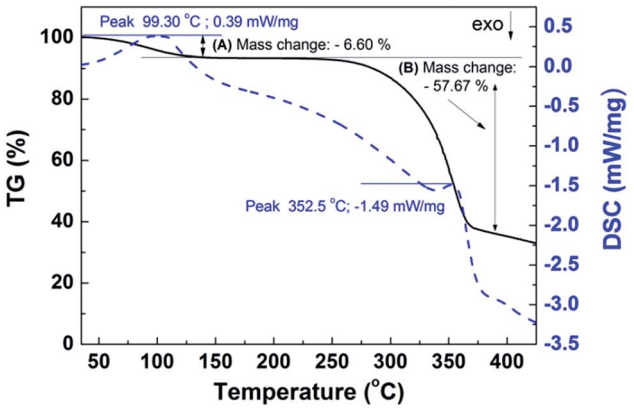

Fig. 3 Temperature-dependent mass change, TG (%), the black line, and heat flux (DSC) signal of cardboard substrate between 40 and 425 °C, as the blue dashed line. "A" and "B" identify the two major mass losses.

obtained by FIB showing the quality and homogeneity of the deposited layers.

A critical technical issue concerns the proper selection of the thickness of the solar cell layers in order to achieve the best performance. Starting with non-optimized conditions, a Design of Experiment (DoE) (see ESI Fig. S2–S4†) study was performed to determine the best combination of layer thicknesses to optimize the solar cell performance. This study led us to select the following thicknesses for the Si layers: n-layer = 30 nm; i-layer = 325 nm; p-layer = 15 nm.

The solar cell deposition process begins with a 60 nm thick interlayer of AZO deposited at 155 °C by RF magnetron sputtering, which contributes to a better optical and electrical matching between the n-layer and the back metal contact, and prevents the diffusion of Al impurities to the silicon layers during the deposition. It is followed by 3 min hydrogen plasma to assure a surface free of contaminants and reactive species for the subsequent deposition of the silicon layers (see Fig. S5 and Table S8 in ESI†).

To ensure the reproducibility of the cells when switching from glass substrate to LPC, a constant monitoring (by OES and QMS) of the reactive species present in the plasma during silicon layers deposition and general contaminants in the PECVD system is required.

Concerning the silicon layers, the intrinsic a-Si:H layer has a photosensitivity ($\sigma_{ph}/\sigma_{d@25\ ^\circ C}$) of 10^7. The degree of compactness of the thin films and structural order, determined by spectroscopic ellipsometry,[27] led to a high Tauc–Lorentz

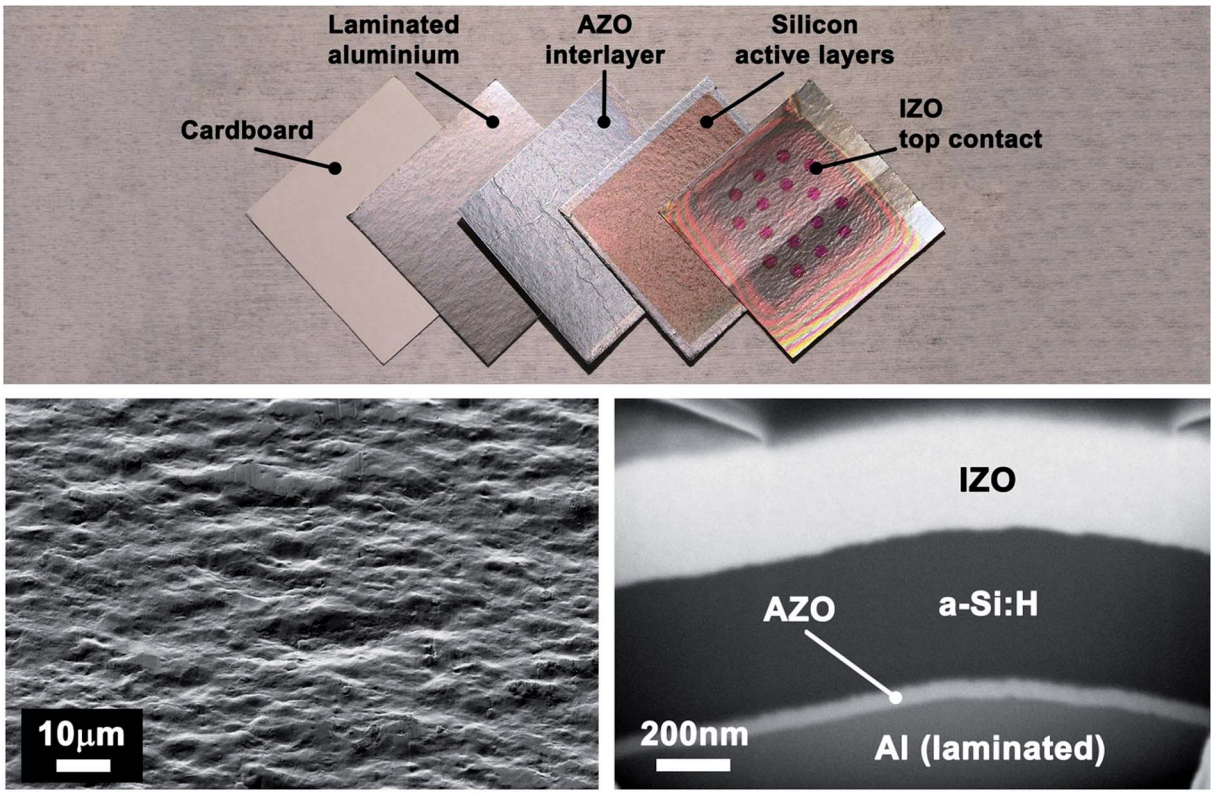

Fig. 4 (a) Image of the different layers that compose the device chronologically ordered from left to right, starting with the cardboard, the aluminium foil laminated with LPDE, which acts as the back contact, the AZO interlayer (~60 nm thickness), the n–i–p silicon layers (~350 nm) and finally the IZO top contact (~300 nm), which also defines the cell area; (b) SEM image of the aluminium surface. One can see a highly rough but defect-free surface; (c) cross-cut FIB image depicting the solar cell layers. The Al (laminated) is a partial cut of the laminated aluminium foil covering the cardboard. The optimized process conditions assure the high conformity of the film to the high substrate roughness and the thickness homogeneity of the layers. The partially peeled layer over the IZO is a protective carbon layer deposited prior to the FIB process to prevent Ga contamination during the etching process.

parameter (A) of 214, which is typical of a compact material, and a low broadening term of the *Lorentz Oscillator* (C) of 2.17, which indicates a high short-distance order. These values are typically attributed to an i-a-Si:H material with good transport properties and low defect density.[27] Regarding the doped layers, p-a-Si:H exhibits $\sigma_{d@25\ ^\circ C} = 1.0 \times 10^{-5}$ S cm^{-1} and $E_a = 0.41$ eV, while n-a-Si:H shows $\sigma_{d@25\ ^\circ C} = 1.9 \times 10^{-2}$ S cm^{-1} and $E_a = 0.17$ eV (see ESI Table S1 and S2†).

Finally, for the top contact, a 300 nm amorphous IZO layer[28] was deposited by RF magnetron sputtering at room temperature. IZO has significant advantages, namely, its highly smooth surface, with outstanding step coverage, transparency (transmittance above 85% in the visible range) and quite low sheet resistance ($\rho = \sim 5 \times 10^{-4}$ Ω cm), for a TCO deposited at room temperature. A mechanical mask was used in order to individualize 16 cells with an area of ~5 mm^2 each (Fig. 1a). Moreover, cells with larger areas of ~20 mm^2 (see the video in ESI†) were also produced at an earlier development stage, showing similar efficiencies.

3.2.1 a-Si:H plasma monitoring by OES. Typical thin film deposition processes on conventional substrates (*e.g.* glass, silicon wafers, *etc.*) can be straightforwardly performed by repeating a pre-optimized step list, since the properties of their materials remain practically unaltered. However, a well-controlled deposition on organic-based substrates like paper, whose composition can be *a priori* undetailed and mutate along the process, requires a feedback procedure able to constantly monitor the changes occurring in the substrate and adapt the deposition conditions accordingly. In this section and in the ESI,† we present a set of essential monitoring techniques and the first steps that, according to the authors, are crucial to define a dynamic deposition methodology enabling the reproducible fabrication of solar cells on paper based substrates.

The simplicity of the setup and its non-interference with plasma makes OES a useful tool that can provide valuable information about the film forming precursors and radicals present in the plasma.[29–32]

Table 1 presents the intensity peaks ratio of the plasma during the deposition of intrinsic thin film on LPC and Al coated glass. Since the interpretation of the measured spectra relies on the relative properties of the plasma, the conclusions are drawn from the ratios of two measured intensity emission lines (or peaks), I_x/I_y, where "I" refers to the optical emission intensity between the upper and the lower states of transition and "x" and "y" are the corresponding atoms or molecules (more information can be found in ESI Fig. S1†).

The identified spectral lines of main interest are the following: Si* ($3s^2 3p^2\ ^1D\ 2 \rightarrow s^2 3p 4s^1 P^0\ 1$) detected at 288 nm,[33] SiH* ($X^2\Pi \rightarrow A^2\Delta$ band), detected at 414 nm,[33] Balmer H_α ($n = 3 \rightarrow n = 2$) detected at 656 nm,[32] and H_β ($n = 4 \rightarrow n = 2$), detected at 486 nm.[32]

It can be noted that the spectral lines associated with oxygen contaminations, namely, oxygen-related transitions, can be detected in the spectrum range from 712 to 780 nm,[34] atomic oxygen spectral lines can be found at 777 and 844 nm, and molecular O_2^* bands at 526, 559, and 599 nm[35] and carbon contamination, such as CH* radiation, detected at 431 nm.[36]

Table 1 OES peaks ratio under study for the i-, n- and p-type layers deposited on glass (coated with Al or corning glass) and LPC. I_{H_β}/I_{H_α} is the ratio between α and β hydrogen emissions; I_{H_α}/I_{SiH^*} ratio between H_α and SiH* optical-emission intensities; I_{Si^*}/I_{SiH^*} intensity ratio of silicon growth precursors Si* and SiH*; I_{O^*}/I_{Si^*} is the ratio between oxygen and silicon optical emission intensities

		Ratio			
Layer	Substrate	I_{H_β}/I_{H_α}	I_{H_α}/I_{SiH^*}	I_{Si^*}/I_{SiH^*}	I_{O^*}/I_{Si^*}
n-layer	Glass/Al	0.57	0.51	0.176	0.21
	LPC	0.57	0.50	0.175	0.21
i-layer	Corning (200 °C)	0.58	0.61	0.197	0.34
	Corning (145 °C)	0.57	0.56	0.175	0.22
	Glass/Al	0.55	0.58	0.162	0.18
	LPC	0.54	0.59	0.157	0.20
p-layer	Glass/Al	0.90	0.27	0.166	0.16
	LPC	0.91	0.27	0.167	0.15

Moreover, to rule out the possible contaminations arising from the substrate and/or the reactor walls and to verify the influence of temperature, OES spectra of i-layer deposition were also recorded after cleaning the reactor at 145 and 200 °C, on corning glass.

Regarding possible contaminants, namely, carbon and oxygen species, OES is not sensible enough to provide qualitative conclusions. Carbon emission is not observed and oxygen related peaks can be detected, but without significant difference between the glass deposited with Al and the LPC substrate. A decrease in the I_{O^*}/I_{Si^*} ratio is observed for all investigated substrates from the first layer deposited (n-layer) to the last one (p-layer).

Given the fact that H_α and SiH* optical emission intensities indicate the amount of atomic H and growth precursor SiH_n ($n = 1, 2, 3$),[37] respectively, the ratio I_{H_α}/I_{SiH^*} provides a quantitative measure of the relative concentration of atomic H and SiH_n precursors in the plasma.[38] Though the ratio I_{H_α}/I_{SiH^*} does not vary significantly between glass/Al and LPC, in the case of the i-layer deposition over glass at 145 °C, I_{H_α}/I_{SiH^*} is slightly lower, which correlates with the higher deposition rate of silicon films grown on glass/Al and LPC substrates. Such variation occurs due to the glass smoothness, where a lower surface area leads to a decrease of the SiH_x precursor's adsorption probability. The intensity of SiH* (I_{SiH^*}) can also be used to infer the deposition rate, since an increase of the SiH* intensity indicates a higher rate;[33] such parameter control is essential when producing solar cells.[39]

The intensity ratios, I_{H_β}/I_{H_α}[39–41] and I_{Si^*}/I_{SiH^*},[42,43] also provide information on electron temperature (T_e). Since T_e is also sensitive to the gas temperature in the plasma, a higher temperature leads to a decrease of the molecular density and elongation of inter-molecular distance for the acceleration of electrons in the plasma and consequently higher T_e.[44] The low deposition temperature of the solar cells (145 °C, below the optimum substrate temperature, which is around 200 °C for amorphous silicon[45]), disturbs the balance between the diffusion length of the growth precursors and the hydrogen evolution on the growing surface. Such facts, in addition to the

higher roughness of coated glass and LPC, help to understand why the corning substrate shows a higher intensity ratio.

3.2.2 MQS monitoring during substrate residence time in PECVD. Quadrupole Mass Spectrometry (QMS) is a useful tool to analyze plasma since it provides complete information about the gas phase chemical composition. The PECVD production process comprises several steps and due to the exotic substrate used in this study, diverse molecules and contaminants can be present and contribute differently to the involving atmosphere. Thus, QMS data were collected for depositions on LPC on several stages, described in Fig. 5. For comparison and control, the signal of a glass substrate after 2 h of pumping and baking was also collected to establish correlation with the possible contaminants present during solar cell production (Fig. 6). The sum of all the identified peaks partial pressure corresponds to more than 98% of the exhaust gas composition (the complete list of identified species can be found in ESI (Fig. S6†), giving us a realistic overview of the ions/molecules present in the chamber during the production stages of the solar cell active layers. The remaining 2% are the sum of the relative pressures below 10^{-10} mbar.

The analysis of the solar cell production stages (Fig. 5) shows the importance of the vacuum pumping time prior to the deposition since it is responsible for the significant reduction of oxygen and water related species (the partial pressure of such air molecules decreases around 25%). Nevertheless, such contaminants are present during the entire process, attesting the large quantities of water adsorbed on the stainless-steel reactor walls[46] and minute leaks.

During pumping, species with higher atomic mass show a constant partial pressure or even exhibit a small increase. Such increase of species in the mass range of 26–45 amu is related with carboxyl and organic compounds (C_xH_y),[46–51] arising from cellulose and LPDE due to thermal degradation.[24,25,52] This effect

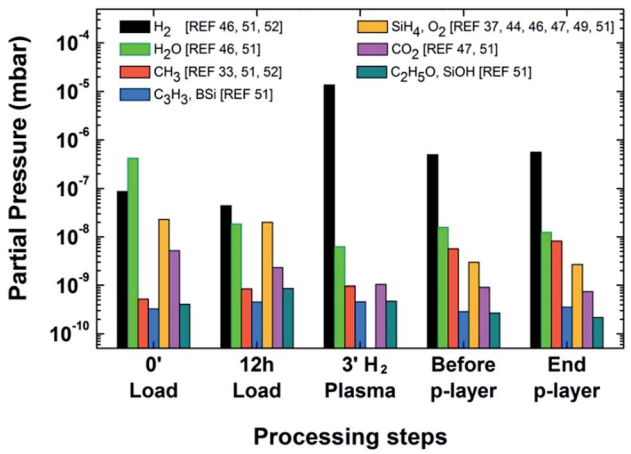

Fig. 5 Partial pressure histograms of the relevant species identified for the different stages of the silicon layers deposition, namely, immediately after loading the substrate in the PECVD system (0′ load), after 12 h of vacuum pumping and baking at 145 °C (12 h load), at the end of the initial 3′ H_2 cleaning plasma (3′ H_2 plasma), before starting the deposition of the p-layer and with stabilized pressure (Before p-layer) and at the end of the p-layer deposition (end p-layer).

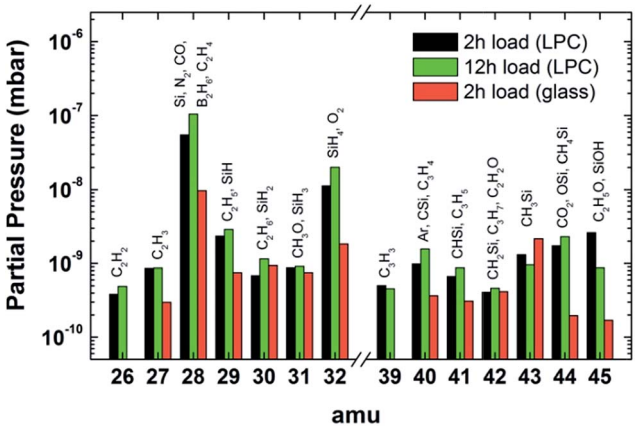

Fig. 6 Comparison between LPC and glass substrate partial pressure histograms of the 26–45 amu signals during the pumping and baking (145 °C). For LPC, two instants are depicted: 2 h of vacuum pumping and baking at 145 °C after loading the substrate in the PECVD, in black, and the signals evolution after 12 h of vacuum pumping and baking at 145 °C (12 h load), in green. In red is the glass sample under the same baking conditions and by pumping during 2 h.

can be observed in Fig. 6, as there are several species after two hours of vacuum pumping and baking, in the case of the LPC, they have partial pressure higher compared to the glass substrate. Thus, such peaks show a significant contribution of carbon species to the partial pressure. The most evident cases are 26 (C_2H_2),[53,54] 28 (N_2, CO, C_2H_4),[46–50,53,54] 32 (O_2),[46,48,49,51,53] 39 (C_3H_3),[53] 44 (CO_2)[49,53] and 45 amu (C_2H_5O),[53] which are the products of thermal degradation of the cellulose and LDPE.[24,52,55] At low temperatures, the thermal degradation of cellulose evolves with dehydration as it leads to depolymerization and dehydrocellulose,[24,52] which ultimately yields volatile compounds (carboxyl and carbonyl groups, CO and CO_2) and char,[26] also confirmed by the constant contribution of CO_2 to the total pressure after 12 h of pumping and throughout the silicon layers deposition.

The fact that the LPC substrate becomes slightly brownish after solar cell deposition is also indicative of the pyrolysis taking place, while LDPE, a thermoplastic made from the monomer ethylene (C_2H_4), produces a wide range of alkanes, alkenes and other species due to the breaking of weak bonds, such as oxygen, incorporated into the main chain as impurities.[24] Despite the fact that decomposition starts around 200 °C at air atmosphere, wherein the polymer is subject to vacuum, the solid–liquid phase transition shifts to lower temperatures[56] leading to such degradation. The evolution of the amu signals with time (from 2 h to 12 h, for LPC) can be observed in Fig. 6, which shows a slight but clear increase; hence the substrate thermal stability under vacuum is inversely proportional to the pumping time and baking temperature.

In addition, peaks that present similar values for the glass substrate (with a stable signal over time) and partial pressure around 10^{-9} mbar (wherein the presence of such organic molecules is not expected at all) can derive from the silicon species, namely, 30 (SiH_2), 31 (SiH_3) and 43 (CH_3Si) degassing from the reactor walls.[48] The H_2 plasma reacts with species on

the chamber walls and those released due to degassing, hence a decrease in partial pressure for higher mass molecules is observed. Nonetheless, the consumption of such molecules leads to an increase of the lower mass reactive species as reaction products that will lead to the incorporation of carbon in the AZO/n-a-Si:H interface, thus contributing to the observed decrease in the solar cell current density (J_{SC}) compared to the same solar cell deposited on glass (Fig. 7a).

3.2.3 Solar cell characterization. Taking into consideration the physical and thermal effects that the deposition process has on the LPC, it was possible to achieve a good compromise of low temperature, gas flows, power density and growth rate to obtain homogeneous layers, and through an extensive analysis of plasma monitoring assure the reproducibility of the characteristics of the layers, namely, thickness, electro and optical properties.

With the deposition process optimized, the best initial value for the a-Si:H solar cells on LPC has a 4.08% efficiency, FF = 53.7%, $J_{SC} = 9.05$ mA cm^{-2} and $V_{OC} = 0.84$ V (Fig. 7 and Table 2). It can be noted that the deposition of the AZO interlayer at a high temperature (155 °C) considerably improves the solar cells, leading to a performance similar to the cells on conventional glass substrates. This can be attributed to the temperature-induced high-strain stresses on the substrate during the deposition processes,[57] meaning that the LDPE loses its rigidity when subjected to $\gtrsim$100 °C temperatures and, together with vacuum, makes the laminated aluminium crease. Thus, by allowing this conformation to take place before the silicon layers deposition, the mechanical deformations are lower and the mismatch between thermal expansion coefficients of the substrate and film decreases.[57]

The external quantum efficiency (EQE) measurements depicted in Fig. 7b for solar cells on glass and the LPC show that the main portion of the photocurrent is produced in the wavelength range between 450 and 550 nm. Above 550 nm, the light traverses the Si layers and is reflected back to the cell by the Al rear contact, thereby forming interferences within the thin Si film, which gives rise to the EQE peaks observed in the longer wavelength region (550–675 nm).[58]

Table 2 Comparison of the solar cell properties deposited on glass and LPC substrates; η, efficiency; FF, fill factor; J_{SC}, short-circuit current density; V_{OC}, open-circuit voltage

Solar cell (substrate)	η (%)	FF (%)	V_{OC} (V)	J_{SC} (mA cm^{-2})	R_S (Ω cm)	R_{Sh} (Ω cm)
LPC (AZO @RT)	3.98	60.1	0.82	8.08	23	984
LPC (AZO @155 °C)	4.08	53.7	0.84	9.05	31	831
Glass (AZO @RT)	4.33	53.3	0.85	9.55	21	446

Furthermore, the number of working cells attained in this substrate is similar to the one on glass, nearly 100%, over the working area of 25 × 25 mm. Since LPC is flexible and the solar cells can resist some degree of paper bending (radius of ~5 mm) with a minimal effect on their performance, ~2% variation of the initial value, it evidences the suitability of LPC as a substrate for a-Si:H cell deposition. The resistance of inorganic TCOs and a-Si:H on flexible substrates (cellulose[59] and polymeric substrates[60]) has been previously demonstrated with films deposited under similar conditions and techniques, showing excellent electrical performances even at a bending radius of 5 mm for TFTs[61] and 20 mm for a-Si:H PV modules over more than 800 bending cycles.[60]

Certain process-related factors have limited the efficiencies attained in this study (~4%), reported in Table 2, namely, the low production temperature and possible cross contamination, due to the Si deposition in a single PECVD chamber, as opposed to a multi-chamber system, which could lead to improvements of above 30%. Nevertheless, the solar cells performance on standard glass and on LPC has demonstrated to be remarkably

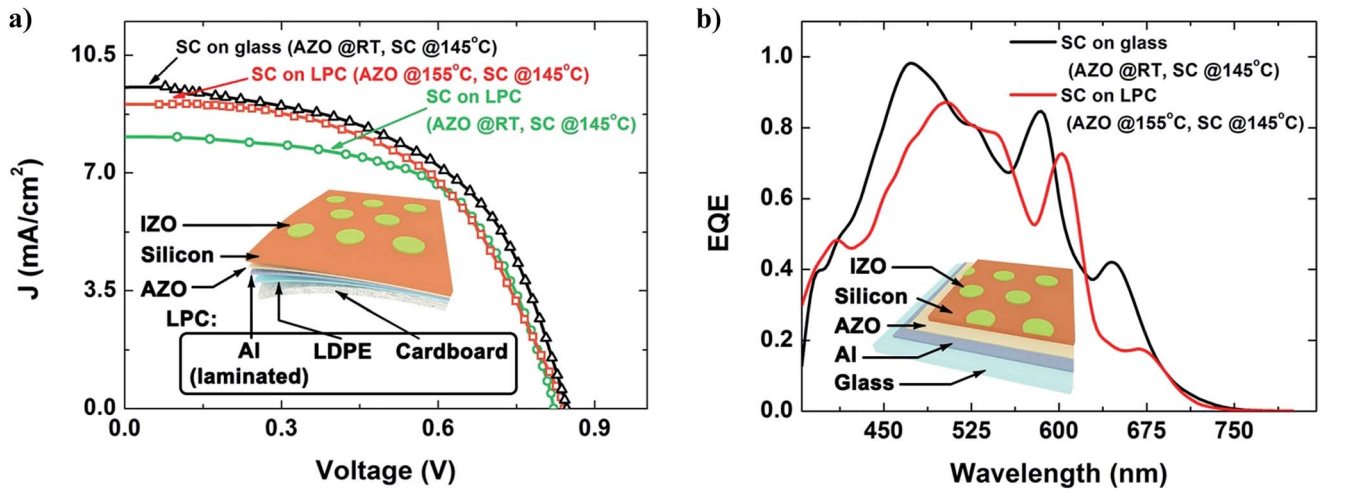

Fig. 7 Performance of a-Si:H solar cells (SCs) deposited on glass and LPC. (a) J–V curves. For the LPC substrate, two different process temperatures were used for the AZO interlayer (room temperature and 155 °C), while the SC Si layers were always deposited at 145 °C. The inset shows the device structure used in this study, wherein the LPC comprises the 3 layers: cardboard, LDPE and laminated Al; (b) External Quantum Efficiency (EQE) of the SC on glass and the best LPC under the same deposition conditions. The inset shows the glass reference device structure.

similar. The slightly lower efficiency of the cells deposited on LPC is expected, since for flexible substrates the deformation induces an accumulation of mechanical stresses (compressive and tensile), which leads to a higher defect density.[66]

Concerning the estimated devices durability, given the type of indoor applications and the expected time frame of utilization around one year, for a-Si:H cells deposited on the onset of crystallinity and with comparable ratio $R = H_2/SiH_4 = 4$, the degradation after 1000 h under $3000l \times (1\ mW\ cm^{-2})$ of a typical indoor spectrum of a F12 fluorescent lamp (with significant UV component) is less than 10%.[60] The devices analysed in this study have been able to endure indoor environmental conditions for a prolonged time and after 14 months they still show comparable efficiencies. Therefore, such light-induced degradation is not expected to hinder their application in low cost sustainable commodities. Moreover, a-Si:H cells have the advantage of a high absorption coefficient (10^4 to 10^5 cm^{-1}) in the visible range and can absorb diffused light, which means that these cells are capable of generating voltages close to their characteristic V_{OC} under typical indoor ambient light conditions.[67]

To better understand the applicability of these solar cells on LPC, it can be compared with the power generated by a commercial printed battery, as that of Enfucell, which already has a wide range of applications, from transdermal delivery patches to wireless–BLE–sensor tags.[68] The SoftBattery Reg 1.5V (Plus) from Enfucell can supply 1.5 V and 8–10 mA on an area of 60 × 72 mm. With the proof of concept solar cells presented herein, it is possible to achieve a similar output over an area of 30 × 20 mm by arranging two rows, each with three cells in series, connected in parallel. This arrangement can output ~2 V and ~15 mA, which shows the potential impact of the devices developed in this study.

4. Cost estimation of the industrial manufacturing of solar cell on packaging cardboard

Accessing the economic viability of LPC as a solar cell substrate for indoors applications helps to put in perspective its relevance and understand why it is important to tackle the emerging field for intelligent packaging and low power disposable consumer electronics. One of the foremost advantages is the fact that the infrastructure and equipment involved in the production of these devices not only matches that one commonly used today in 2nd generation solar cell production, but it is also compatible with the roll-to-roll technology,[69] which is the preferred manufacturing process in packaging industry. Thus, no extra major capital expenses in terms of manufacturing equipment are required.

To perform the cost-effectiveness analysis presented next (Table 3 and Fig. 8), LPC is compared with three other viable substrates for flexible solar cells, namely, PEN/PET, stainless steel[64] and a recent technology, flexible glass.[70] In addition to the inexistence of extra capital cost for the construction/adaptation of a production unit, the following two assumptions are made: (1) since only the production process is being considered and not the end user applications, the calculations will be done solely for the solar cell production and not for the process that comes after the solar cell deposition (namely, mounting, wiring, equipment and other capital costs). This way, the influence arising from the substrate in the final expenditure can be highlighted. (2) Regarding encapsulation, paper based solar cells, besides the typical encapsulation process used in flexible solar cell for higher protection, LPC can undergo a cheaper one, considering the final LDPE protective layer applied in the cardboard packaging industry.

Table 3 describes all the costs ($ per m^2) related to material and processes for a low/optimum estimated cost and possible high end of price range. Price estimations and calculations are presented elsewhere,[65] unless described otherwise. Electricity generated as $ per Wp is calculated by dividing the manufacturing cost ($ per m^2) by the output of the same area (1000 Wp m^{-2}) times efficiency. Assuming a module efficiency equal to the present 4% solar cell efficiency, the manufacturing cost will be between $0.38 per Wp for the optimum price estimative, and $2.04 per Wp for an estimation of the upper price range. Fig. 8 helps to visualize the material cost distribution for the lower estimated values, and compare the impact that the different substrates have in the final value. Since LPC has the lowest substrate cost, the manufacturing cost is significantly reduced, despite the considered 20% higher silicon thin film process cost.

Considering the cost of paper-based PV, the LPC falls in an economically viable price range. However, even assuming a small increase in efficiency up to 5%, which Brinza *et al.* were able to achieve for 100 °C on stainless steel foil,[71] and assuming a module efficiency equal to the cell efficiency, the manufacturing cost will drastically reduce to $0.31–1.64/Wp (optimum and high estimative), giving LPC a competitive price for low cost PV.

5. Sustainability and recyclability of solar cells on packaging cardboard

Regarding the recyclability of solar cells on LPC substrates, the cardboard packaging industry already has a mature recycling process,[72] briefly, it consists of mixing the packaging cardboard with water; the wood fibres separate from LDPE and aluminium, allowing paper pulp to be reused and the mixture LDPE/Al to be turned into new products.[73] The added value that a solar cell can bring will not hinder that fact, since the quantity of active semiconductor material in the cell is extremely small. In fact, recently, paper mills are also applying pyrolysis to separate the LPDE and Al (poly-al) by heating up to 500 °C without oxygen. This way, the plastics do not burn and the evaporated gas by product is used to generate electricity and steam, and the resulting Al has a high-grade purity.[74]

Concerning the solar cell material, the a-Si:H has a suitable relation in terms of environmental impact *vs.* production cost[75] compared with most photovoltaic materials. The pay-off time for the present devices is estimated to be in the range of 0.4–2

Table 3 Material cost distribution of a-Si:H solar modules on LPC, PEN/PET, stainless steel and flexible glass per square meter (cost, $ per m^2). "Low" column relates to an optimum estimative, while the "High" column considers the upper limit of the price range

		LPC		PEN/PET		Stainless steel		Flexible glass	
Cost component		Low	High	Low	High	Low	High	Low	High
Antireflection layer		1.2[a]	6.0[a]	1.0	5.0	1.0	5.0	1.0	5.0
Top contact (TCO)		2.0	5.0	2.0	5.0	2.0	5.0	2.0	5.0
Bottom contact (metal/TCO)		N/A[b]	N/A[b]	2.0	5.0	N/A	N/A	2.0	5.0
Electrical contacts and interconnects		2.9	6.0	2.9	6.0	2.9	6.0	2.9	6.0
Encapsulant		0.1[c]	4.4[d]	2.9	4.4	2.9	4.4	1.9	5.5
Sealant		0.1	4.4	2.9	4.4	2.9	4.4	3.6	5.4
Thin film Si[e]	Material	2.0	30.0	2.0	30.0	2.0	30.0	2.0	30.0
	Energy	1.8[f]	6.0[f]	1.5	5.0	1.5	5.0	1.5	5.0
	Process	3.0[f]	14.4[f]	2.5	12	2.5	12.0	2.5	12.0
	Maintenance	1.8[f]	4.8[f]	1.5	4.0	1.5	4.0	1.5	4.0
Effective total		14.9	81.0	21.2	80.8	19.2	75.8	20.9	82.9
Substrate		0.5[g]	0.8[h]	5.0[i]	8.0[j]	4.0[k]	4.0	7.5[l]	20.0
Total		15.4	81.8	26.2	88.8	23.2	79.8	28.4	102.9

[a] An extra cost of 20% is considered since the deposition process requires temperature to assure proper degassing and decrease adhesion stress. [b] Not applied. The LPC and stainless steel substrates already encompass the bottom contact. [c] Estimated from the substrate industrial cost. Considering the composition fractions of the total substrate, LDPE accounts for 20%, which provides a rough estimation of the encapsulation cost. [d] Considering the high cost for encapsulating a flexible SC (plastic substrate). [e] High end price also considers the increase in cost in the case of a double junction solar cell. [f] The costs were increased by 20% due to higher consumption of energy, processing and maintenance compared with other substrates, resulting from the increased pumping time and reactor cleaning. [g] Value provided by the packaging industry. [h] Value estimated for the end-user. [i] Kalowekano *et al.* (2009).[62] [j] Krebs *et al.* (2010).[63] [k] Brown *et al.* (2014).[64] [l] Value estimated from industrial glass[65] plus 25% to compensate handling, transportation and usage, since flexible glass is highly susceptible to breaking and cracking along the edges if even slightly mishandled.

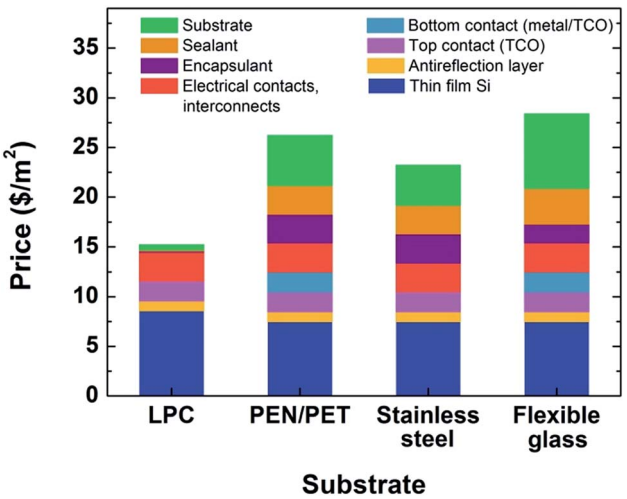

Fig. 8 Manufacturing cost ($ per m^2) comparison between LPC, PEN/PET, stainless steel and flexible glass.

years, assuming large-scale roll-to-roll manufacturing processes, which is comparable to the lifetime of several disposable packaging applications.

6. Conclusions and challenges for future development

In the present study, the viability of fabricating a-Si:H solar cells at low temperature, with an efficiency of 4%, on liquid packaging cardboards is demonstrated for the first time, to the authors' knowledge. This process naturally incorporates a high quality Al back contact compatible with the silicon thin film deposition conditions by PECVD. A working device can be seen in the ESI Video.† The potential of our technology could only be attained after proper improvement of the process parameters, such as a special control of the process gas dilution, the systematic study of doping from gas phase,[76] hydrogen plasma treatment (see ESI Fig. S5†) and the fabrication of n–i–p junctions and contacts with the adequate layer thicknesses and electro-optical characteristics;[77,78] together with studies devoted to process monitoring and interface quality improvement, which proved to be highly relevant.

Moreover, we identified engineering challenges to improve the device efficiency and throughput that require the use of multi-chamber systems (to avoid cross contaminations and enhance the throughput) and by using effective light trapping schemes, as those based on scattering nanoparticles.[79] Further research on how to improve the LPC integrity is also needed, by optimizing the lamination polymer, LDPE, to seal the cellulose and prevent the loss of water inside the LPC, which is crucial to preserve its intrinsic flexibility and counteract the fragility that the production process can cause on the substrate.[61] Finally, the optimization of the cell production will also address the utilization of In free front TCO. As a critical material, the use of In should not be applied in disposable and low cost applications; nevertheless, the process must be performed at room temperature and exhibit similar performances as the on-going work points out.[80]

The innovation reported herein is a significant step towards an energetic revolution of mobile and intelligent systems by opening the path for several new solar cells applications in low cost disposable products. This can produce a tremendous impact on today's existing smart packaging industry and promote spin-offs towards other relevant fields of mobile systems, disposable electronics and smart textiles.

Acknowledgements

This study was funded by the Portuguese Science Foundation (FCT-MEC) through the projects EXCL/CTM-NAN/0201/2012, UID/CTM/500025/2013 and the A3Ple (FP7, NMP-2010-SME-4 grant 262782). Moreover, this study was also supported by E.F.'s ERC 2008 Advanced Grant (INVISIBLE contract number 228144). The authors want to thank their colleagues Daniela Gomes for SEM images acquisition, Rita Branquinho for helping with 3D profilometer, Alexandra Gonçalves for STA measurements and Manuel J. Mendes for revising the manuscript. A.V. acknowledges the support from the Portuguese Foundation for Science and Technology (FCT) and MIT-Portugal through the scholarship SFRH/BD/33978/2009.

Notes and references

1 M. Berggren, D. Nilsson and N. D. Robinson, *Nat. Mater.*, 2007, **6**, 3–5.
2 R. Martins, I. Ferreira and E. Fortunato, *Phys. Status Solidi RRL*, 2011, **5**, 332–335.
3 R. F. P. Martins, A. Ahnood, N. Correia, L. Pereira, R. Barros, P. Barquinha, R. Costa, I. M. M. Ferreira, A. Nathan and E. Fortunato, *Adv. Funct. Mater.*, 2013, **23**, 2153–2161.
4 K. L. Yam, P. T. Takhistov and J. Miltz, *J. Food Sci.*, 2005, **70**, R1–R10.
5 N. Sozer and J. L. Kokini, *Trends Biotechnol.*, 2009, **27**, 82–89.
6 C. M. Lopes, J. R. Fernandes and P. Martins-Lopes, *Food Technol. Biotechnol.*, 2013, **51**, 183–197.
7 R. J. Lehmann, R. Reiche and G. Schiefer, *Comput. Electron. Agr.*, 2012, **89**, 158–174.
8 D. A. Pereira de Abreu, J. M. Cruz and P. Paseiro Losada, *Food Rev. Int.*, 2011, **28**, 146–187.
9 A. P. F. Turner, *Chem. Soc. Rev.*, 2013, **42**, 3184–3196.
10 Y. G. Sun and J. A. Rogers, *Adv. Mater.*, 2007, **19**, 1897–1916.
11 N. P. Mahalik and A. N. Nambiar, *Trends Food Sci. Technol.*, 2010, **21**, 117–128.
12 D. Tobjork and R. Osterbacka, *Adv. Mater.*, 2011, **23**, 1935–1961.
13 H. E. Nilsson, T. Unander, J. Siden, H. Andersson, A. Manuilskiy, M. Hummelgard and M. Gulliksson, *IEEE Trans. Compon., Packag., Manuf. Technol.*, 2012, **2**, 1723–1734.
14 H. Cortina, C. Martínez-Alonso, M. Castillo-Ortega and H. Hu, *Mater. Sci. Eng. B*, 2012, **177**, 1491–1496.
15 Y. H. Zhou, C. Fuentes-Hernandez, T. M. Khan, J. C. Liu, J. Hsu, J. W. Shim, A. Dindar, J. P. Youngblood, R. J. Moon and B. Kippelen, *Sci. Rep.*, 2013, **3**, 1536.
16 M. L. Brongersma, Y. Cui and S. Fan, *Nat. Mater.*, 2014, **13**, 451–460.
17 Z. Fan, H. Razavi, J.-W. Do, A. Moriwaki, O. Ergen, Y.-L. Chueh, P. W. Leu, J. C. Ho, T. Takahashi, L. A. Reichertz, S. Neale, K. Yu, M. Wu, J. W. Ager and A. Javey, *Nat. Mater.*, 2009, **8**, 648–653.
18 M. Kaltenbrunner, T. Sekitani, J. Reeder, T. Yokota, K. Kuribara, T. Tokuhara, M. Drack, R. Schwodiauer, I. Graz, S. Bauer-Gogonea, S. Bauer and T. Someya, *Nature*, 2013, **499**, 458–465.
19 M. Stuckelberger, Y. Riesen, M. Despeisse, J.-W. Schüttauf, F.-J. Haug and C. Ballif, *J. Appl. Phys.*, 2014, **116**, 094503.
20 M. C. Barr, J. A. Rowehl, R. R. Lunt, J. J. Xu, A. N. Wang, C. M. Boyce, S. G. Im, V. Bulovic and K. K. Gleason, *Adv. Mater.*, 2011, **23**, 3500–3505.
21 S. Roy, R. Bajpai, A. K. Jena, P. Kumar, N. kulshrestha and D. S. Misra, *Energy Environ. Sci.*, 2012, **5**, 7001–7006.
22 Stora Enso, http://www.storaenso.com/.
23 S. Morawiec, M. J. Mendes, S. A. Filonovich, T. Mateus, S. Mirabella, H. Águas, I. Ferreira, F. Simone, E. Fortunato, R. Martins, F. Priolo and I. Crupi, *Opt. Express*, 2014, **22**, A1059–A1070.
24 S. o. F. P. E. National Fire Protection Association, *SFPE handbook of fire protection engineering*, National Fire Protection Association; Society of Fire Protection Engineers, Quincy, Boston, Mass., 1995.
25 T. Andersson, B. Stålbom and B. Wesslén, *J. Appl. Polym. Sci.*, 2004, **91**, 1525–1537.
26 Alternative pathways for pyrolysis of cellulose, ACS National Meeting, Washington, D.C., 1983, Amer Chemical Soc, 285–290.
27 H. Águas, V. Silva, E. Fortunato, S. Lebib, P. R. I. Cabarrocas, I. Ferreira, L. Guimarães and R. Martins, *Jpn. J. Appl. Phys.*, 2003, **42**, 4935.
28 P. Barquinha, G. Goncalves, L. Pereira, R. Martins and E. Fortunato, *Thin Solid Films*, 2007, **515**, 8450–8454.
29 S. Muthmann and A. Gordijn, *Sol. Energy Mater. Sol. Cells*, 2011, **95**, 573–578.
30 J. K. Rath, M. Brinza, Y. Liu, A. Borreman and R. E. I. Schropp, *Sol. Energy Mater. Sol. Cells*, 2010, **94**, 1534–1541.
31 L. Shui-Yang, C. Yu-Cheng, C. Yun-Shao, C. Yin-Yu and L. Shuo-Jen, *IEEE Trans. Electron Devices*, 2012, **59**, 1245–1254.
32 B. Strahm, A. Feltrin, R. Bartlome and C. Ballif, SPIE conference on Thin Film Solar Technology, San Diego, 2009, 74090E.
33 S.-Y. Lien, Y.-Y. Chang, Y.-S. Cho, J.-H. Wang, K.-W. Weng, C.-H. Chao and C.-F. Chen, *J. Non-Cryst. Solids*, 2011, **357**, 161–164.
34 G.-F. Hou, X.-H. Geng, X.-D. Zhang, J. Sun, J.-J. Zhang and Y. Zhao, *Chin. Phys. B*, 2011, **20**, 077802.
35 E. Vassallo, A. Cremona, F. Ghezzi and D. Ricci, *Vacuum*, 2010, **84**, 902–906.
36 K. Tsuji and K. Hirokawa, *Thin Solid Films*, 1991, **205**, 6–12.
37 J. Ge, Z. P. Ling, J. Wong, R. Stangl, A. G. Aberle and T. Mueller, *J. Appl. Phys.*, 2013, **113**, 234310.

38 Z. M. Wu, J. Sun, Q. S. Lei, Y. Zhao, X. H. Geng and J. P. Xi, *Phys. E*, 2006, **33**, 125–129.
39 J. K. Rath, A. D. Verkerk, Y. Liu, M. Brinza, W. J. Goedheer and R. E. I. Schropp, *Mater. Sci. Eng., B*, 2009, **159–60**, 38–43.
40 Y. Liu, A. D. Verkerk, J. K. Rath, R. E. I. Schropp and W. J. Goedheer, in *Physica Status Solidi C - Current Topics in Solid State Physics*, ed. R. E. I. Schropp, 2010, vol. 7, no. 3-4, pp. 575–578.
41 K. Saito and M. Kondo, *Phys. Status Solidi A*, 2010, **207**, 535–538.
42 Y.-S. Lee, J.-H. In, S.-K. Ahn, S.-H. Seo, H.-Y. Chang, D.-J. You, S.-W. Ahn and H.-M. Lee, *Curr. Appl. Phys.*, 2010, **10**, S234–S236.
43 M. Takai, T. Nishimoto, M. Kondo and A. Matsuda, *Sci. Technol. Adv. Mater.*, 2001, **2**, 495–503.
44 Y. Sobajima, T. Higuchi, J. Chantana, T. Toyama, C. Sada, A. Matsuda and H. Okamoto, in *Physica Status Solidi C – Current Topics in Solid State Physics* , ed. R. E. I. Schropp, 2010, vol. 7, no. 3-4, pp. 521–524.
45 A. Matsuda, *Jpn. J. Appl. Phys., Part 1*, 2004, **43**, 7909–7920.
46 H. A. Weakliem, R. D. Estes and P. A. Longeway, *J. Vac. Sci. Technol., A*, 1987, **5**, 29–36.
47 A. I. Chowdhury, T. M. Klein, T. M. Anderson and G. N. Parsons, *J. Vac. Sci. Technol., A*, 1998, **16**, 1852–1856.
48 O. Gabriel, S. Kirner, M. Klick, B. Stannowski and R. Schlatmann, *EPJ Photovoltaics*, 2014, **5**, 55202.
49 S. Kirner, O. Gabriel, B. Stannowski, B. Rech and R. Schlatmann, *Appl. Phys. Lett.*, 2013, **102**, 051906.
50 S. Xu, X. Zhang, Y. Li, S. Xiong, X. Geng and Y. Zhao, *Thin Solid Films*, 2011, **520**, 694–696.
51 T. Nishimoto, M. Takai, H. Miyahara, M. Kondo and A. Matsuda, *J. Non-Cryst. Solids*, 2002, **299–302**(2), 1116–1122.
52 I. Milosavljevic and E. M. Suuberg, *Ind. Eng. Chem. Res.*, 1995, **34**, 1081–1091.
53 NIST Standard Reference Data, http://webbook.nist.gov/chemistry/mw-ser.html.
54 I. Ferreira, V. Silva, H. Águas, E. Fortunato and R. Martins, *Appl. Surf. Sci.*, 2001, **184**, 60–65.
55 R. Martins, P. Barquinha, L. Pereira, N. Correia, G. Gonçalves, I. Ferreira and E. Fortunato, *Appl. Phys. Lett.*, 2008, **93**, 203501–203504.
56 V. V. Brazhkin and A. G. Lyapin, *Nat. Mater.*, 2004, **3**, 497–500.
57 Y. Li and D. Du, *Characterization of Low Temperature Deposited Flexible Amorphous Silicon Solar Cells*, 2009.
58 J. K. Rath, M. Brinza and R. E. I. Schropp, in *2009 34th IEEE Photovoltaic Specialists Conference*, Ieee, New York, 2009, vol. 1–3, pp. 1743–1746.
59 R. Martins, A. Nathan, R. Barros, L. Pereira, R. Barquinha, N. Correia, R. Costa, A. Ahnood, I. Ferreira and E. Fortunato, *Adv. Mater.*, 2011, **23**, 4491–4496.
60 M. Foti, C. Tringali, A. Battaglia, N. Sparta, S. Lombardo and C. Gerardi, *Sol. Energy Mater. Sol. Cells*, 2014, **130**, 490–494.
61 L. Pereira, D. Gaspar, D. Guerin, A. Delattre, E. Fortunato and R. Martins, *Nanotechnology*, 2014, **25**, 094007.
62 J. Kalowekamo and E. Baker, *Sol. Energy*, 2009, **83**, 1224–1231.
63 F. C. Krebs, T. Tromholt and M. Jorgensen, *Nanoscale*, 2010, **2**, 873–886.
64 T. M. Brown, F. De Rossi, F. Di Giacomo, G. Mincuzzi, V. Zardetto, A. Reale and A. Di Carlo, *J. Mater. Chem. A*, 2014, **2**, 10788–10817.
65 H. Aguas, S. K. Ram, A. Araujo, D. Gaspar, A. Vicente, S. A. Filonovich, E. Fortunato, R. Martins and I. Ferreira, *Energy Environ. Sci.*, 2011, **4**, 4620–4632.
66 E. Fortunato, L. Pereira, H. Aguas, I. Ferreira and R. Martins, *Proc. IEEE*, 2005, **93**, 1281–1286.
67 R. A. Street, *Hydrogenated Amorphous Silicon*, Cambridge University Press, 2005.
68 Enfucell SoftBattery, http://www.enfucell.com/softbattery.
69 S.-F. Leung, L. Gu, Q. Zhang, K.-H. Tsui, J.-M. Shieh, C.-H. Shen, T.-H. Hsiao, C.-H. Hsu, L. Lu, D. Li, Q. Lin and Z. Fan, *Sci. Rep.*, 2014, **4**, 4243.
70 S. M. Garner, H. Mingqian, L. Po-Yuan, S. Chao-Feng, L. Chueh-Wen, H. Yen-Min, R. Hsu, D. Jau-Min, H. Je-Ping, C. Yi-Jen, J. J. ChiehLin, L. Xinghua, M. Sorensen, L. Jianfeng, P. Cimo and C. Kuo, *J. Disp. Technol.*, 2012, **8**, 590–595.
71 M. Brinza, J. K. Rath and R. E. I. Schropp, *Sol. Energy Mater. Sol. Cells*, 2009, **93**, 680–683.
72 A. L. Mourad, E. E. C. Garciaa, G. B. Vilela and F. Von Zuben, *Resour., Conserv. Recycl.*, 2008, **52**, 678–689.
73 M. Grosso, L. Biganzoli and L. Rigamonti, *Resour., Conserv. Recycl.*, 2011, **55**, 1178–1184.
74 *Stora Enso, Rethink "From juice carton to car parts"*, http://www.storaenso.com/rethink/from-juice-carton-to-car-parts.
75 J. M. Pearce and A. Lau, *ASME Solar 2002: International Solar Energy Conference*, 2002, pp. 181–186.
76 Y. Peng, Z. Q. He, A. Diyaf, A. Ivaturi, Z. Zhang, C. J. Liang and J. I. B. Wilson, *Appl. Phys. Lett.*, 2014, **104**, 103903.
77 S. A. Filonovich, H. Águas, T. Busani, A. Vicente, A. Araújo, D. Gaspar, M. Vilarigues, J. Leitão, E. Fortunato and R. Martins, *Sci. Technol. Adv. Mater.*, 2012, **13**, 045004.
78 R. Martins, L. Raniero, L. Pereira, D. Costa, H. Águas, S. Pereira, L. Silva, A. Gonçalves, I. Ferreira and E. Fortunato, *Philos. Mag.*, 2009, **89**, 2699–2721.
79 M. J. Mendes, S. Morawiec, F. Simone, F. Priolo and I. Crupi, *Nanoscale*, 2014, **6**, 4796–4805.
80 P. Barquinha, R. Martins, L. Pereira and E. Fortunato, *Transparent Oxide Electronics: From Materials to Devices*, Wiley, 2012.

